First-principles Investigation of B-site Ordering in $Ba(Mg_x,Ta_{1-x})O_3$ Microwave Dielectrics with the Complex Perovskite Structure

Takeshi TAKAHASHI†, Eric J. WU, Anton VAN DER VEN and Gerbrand CEDER

Department of Materials Science and Engineering, Massachusetts Institute of Technology, 77 Massachusetts Avenue, Cambridge, Massachusetts 02139 U.S.A.

† present address:

Materials Research Center, TDK Corporation, 570-2 Aza-matsugashita, Minami-hatori, Narita, Chiba 286-8588 JAPAN

(Received ; accepted for publication

The B-site cation ordering of $Ba(Mg_{1/3},Ta_{2/3})O_3$ microwave dielectrics with the complex perovskite structure has been studied using a combination of first-principles calculations, a cluster expansion technique, and Monte Carlo simulations. Our calculations confirm the experimentally observed hexagonal superstructure with space group $P\bar{3}m1$ (D^3_{3d}) as the ground state. The order-disorder transition between the low-temperature 1:2 ordered hexagonal phase ($P\bar{3}m1$) and high-temperature simple perovskite phase ($Pm3m$) is predicted to occur at ~ 3770 K. This indicates that $Ba(Mg_{1/3},Ta_{2/3})O_3$ in equilibrium should be fully ordered at all practical temperatures. Sintering at high

temperature for a long time or prolonging the anneal should therefore be effective in enhancing the degree of cation order in $Ba(Mg_{1/3},Ta_{2/3})O_3$. The charge density distribution and one electron density of states (DOS) for the 1:2 ordered structure indicate that Ta and O atoms possess some degree of covalency with some overlap between the O-2*p* orbitals and the Ta-5*d* orbitals.

KEYWORDS: $Ba(Mg_{1/3},Ta_{2/3})O_3$, microwave dielectrics, order-disorder transition, first-principles, cluster expansion, Monte Carlo simulation, charge density distribution, density of states.

1. Introduction

Recently, mobile communications have become widespread, as evidenced by the extensive use of pagers, cellular phones and wireless LANs. When global satellite phones and wideband code division multiple access (W-CDMA) systems are practically introduced, mobile communication requirements will increase even more. The proliferation of Radio Frequency (RF) devices such as band-pass filters, resonators, and oscillators, has generated considerable materials research into the microwave dielectrics present in these devices. These RF systems require low power consumption and narrow frequency selectivity, which are determined by the Q-factor of the dielectric, a measure of the relative absorption in the microwave regime. Thus, it is important to develop and study dielectrics with a high Q-factor in the microwave regime. Other key factors of good microwave dielectrics besides a high Q-factor are high dielectric constant and near-zero temperature coefficient of resonant frequency (TCf).

The complex perovskite $A(B'_{1/3},B''_{2/3})O_3$ ceramics have been widely studied as high Q-factor microwave dielectrics[1-3]. In order to elucidate the mechanisms of dielectric characteristics and increase the accuracy of Q-factor evaluation for these materials, far infrared reflection spectroscopy[4], lattice vibrations[5], phase transitions[6,7], ionic model calculations[8-11] and direct measurement techniques[12-14] have been discussed.

One of these ceramics, $Ba(Mg_{1/3},Ta_{2/3})O_3$ (BMT), is known to possess the highest product of frequency (f) and Q (Qf~430000 GHz), moderate dielectric constant (ε_r~24) and near-zero TCf[15,16]. BMT has been put to practical use as dielectric resonators, oscillators and filters in base stations for the RF range[17].

When Mg and Ta cations are disordered over the B-site, the crystal structure of BMT is a cubic perovskite with Pm3m (O^1_h) space group symmetry. When B-site cations order along the [111] direction of this simple perovskite compound, a hexagonal superlattice is formed with space group

$P\bar{3}m1$ (D^3_{3d}), as illustrated in Figs.1(a)-(c)[18,19]. This ordering has been investigated for its effect on the microwave Q-factor: A strong relationship between ordering parameters and microwave Q-factors in BMT system was experimentally observed by Matsumoto *et al*. under various heat conditions[15]. Kawashima *et al*. reported a remarkable improvement of the microwave Q-factor in the similar $Ba(Zn_{1/3},Ta_{2/3})O_3$ system by prolonged sintering, and indicated that this Q-factor improvement corresponded with an increase in cation order of the structure[2]. A similar sintering effect can be also seen in BMT system[16].

The objective of this paper is to study the order-disorder phenomena of the B-site cations in $Ba(Mg_{1/3},Ta_{2/3})O_3$ using first-principles methods. The cluster expansion method, which can be used to study fully or partially disordered systems, is outlined in the next section. Results are presented and discussed in section 3.

2. Methodology

To examine the B-site ordering in the $Ba(Mg_x,Ta_{1-x})O_3$ system, a generalized lattice model based on the cluster expansion technique is applied[20-24]. The cluster expansion is a method to parameterize the energy of the material as a function of the distribution of Mg and Ta cations over the B-sites. A well-converged cluster expansion can represent the energy of any configuration from fully ordered to fully disordered. This method has been successfully applied to the study of configurational disorder and phase transitions in oxides, metals, and semiconductors[20,21,24,25].

The characterization of a configuration is done with pseudospin variables s_i, assigned to each possible B-site i. The variable s_i is +1 (-1) if a Mg (Ta) atom occupies site i. It has been shown that the configurational energy, *E*, can be exactly expanded in terms of polynomials f_a of these discrete pseudospin variables s_i[20]. f_a is defined as a product of pseudospin variables s_i, s_j, …, s_N, where the

indices i, j, ...,N correspond to a collection of sites belonging to the cluster α. The clusters α can, for example, be a nearest-neighbor pair cluster, a next nearest-neighbor pair cluster, a nearest-neighbor triplet cluster, and so on. The cluster expansion Hamiltonian takes the form:

$$E = V_0 + \sum_a V_a f_a \quad , \qquad \text{(Eq.1)}$$

where

$$f_a = \prod_{i \in a} s_i \quad . \qquad \text{(Eq.2)}$$

V_0 and V_a are constant expansion coefficients and are called the effective cluster interactions (ECI's). The sum in the Eq.1 extends over all possible clusters of B-sites α. However, in practice, Eq.1 can be truncated after some maximal cluster. Numerical values for the ECI can be determined by fitting to calculated energies of a series of structures with different B-site arrangements. A truncated form of Eq.1 was fitted to the values of these energies using linear programming techniques[26] rather than with traditional least squares fitting techniques. Finite temperature information on the structures and thermodynamics is obtained by Monte Carlo simulations on the cluster expansion[27].

An advantage of the cluster expansion formalism is that it can be used with any model for the energy. Using various models that incorporate different interactions can therefore give direct insight into the specific physics, which stabilizes a particular structure.

In this work, we investigate the B-site ordering with an accurate quantum mechanical method, as well as with a simple electrostatic model. For the latter model, Madelung energies were determined for various B-site configurations on a fixed underlying lattice. The objective of using this simple energy model is to investigate which B-site ordering has the lowest electrostatic energy. The form of the electrostatic interaction in this study is a simple Coulomb potential:

$$E = \sum_{i,j}^{N} \frac{q_i q_j}{r_{ij}}, \qquad \text{(Eq.3)}$$

where q represents the charge on the ions and r_{ij} is the distance between ion i and ion j.

Secondly, a more accurate parameterization of the energy of B-site arrangements was obtained with quantum mechanical first-principles methods. Total energies were obtained for a series of B-site ordered superstructures in the $Ba(Mg_x,Ta_{1-x})O_3$ system with the Vienna *Ab initio* Simulation Package (VASP)[28,29]. VASP numerically solves the Kohn-Sham equations within the Local Density Approximation (LDA) using ultra-soft pseudopotentials[30,31] and a plane wave basis set. An energy cutoff of 600 eV was used for the plane wave expansion, since this value was sufficient to ensure convergence of the energy. The exchange and correlation potential implemented in the calculations was that of Ceperley and Alder as parameterized by Perdew and Zunger[32,33]. Cell parameters and positional parameters were fully relaxed for each structure with the conjugate gradient algorithm.

Charge compensation requires Mg and Ta cations to be present in a perfect 1 to 2 ratio. Any deviation from this stoichiometry is expected to occur at a very high energy cost. In order for this energy cost to be well represented by the cluster expansion, it is important to include non-stoichiometric structures in the fit. Hence we calculate not only the energy of $Ba(Mg_{1/3},Ta_{2/3})O_3$ with various B-site configurations, but also that of hypothetical compounds with different ratios of Mg to Ta cations such as $Ba(Mg_{1/2},Ta_{1/2})O_3$, $Ba(Mg_{2/3},Ta_{1/3})O_3$, and so forth. Since no vacancies or interstitials are allowed in our calculations on these non-stoichiometric phases, all charge compensations are forced to occur by valence shifts of the ions. By including these non-stoichiometric compounds in the cluster expansion, it is possible to accurately capture the high energy of ionic arrangements which are locally charge imbalanced.

Rather than plot the total energy of each structure (which is very large), we plot the formation energy, D_fE, which for a given B-site arrangement with composition $Ba(Mg_x,Ta_{1-x})O_3$, is defined as:

$$\Delta_f E_{Ba(Mg_x,Ta_{1-x})O_3} = E - xE_{BaMgO_3} - (1-x)E_{BaTaO_3} \quad , \qquad \text{(Eq.4)}$$

where E is the total energy of the configuration per $Ba(Mg_x,Ta_{1-x})O_3$ formula unit, and E_{BaMgO3} and

E_{BaTaO3} are the energies of the hypothetical $BaMgO_3$ and $BaTaO_3$ perovskites. Subtracting or adding a linear function of composition from the energies does not modify any equilibria between structures. In this case, the hypothetical end-members, $BaMgO_3$ and $BaTaO_3$, were used for convenience only.

3. Results and discussion

3.1. Electrostatic energy

The calculations of the electrostatic energy have been carried out for all possible B-site configurations of $Ba(Mg_{1/3},Ta_{2/3})O_3$ in unit cells with up to 75 atoms. These 2194 different supercells include three structures with 3 B-sites in the unit cell (15 atoms), twenty-four structures with 6 B-sites (30 atoms), fifty-two structures with 9 B-sites (45 atoms), seven-hundred-twenty-three structures of 12 B-sites (60 atoms), and one-thousand-three-hundred-ninety-two structures of 15 B-sites (75 atoms).

The crystal structures of the supercells with the four lowest electrostatic energies are illustrated in Fig.2. The B-site configurations for these structures are shown in Figs.3(a)-(d). These results indicate that the experimentally observed structure is also the one with lowest electrostatic energy, in agreement with an earlier Monte Carlo simulation by Bellaiche *et al*[11].

The electrostatic ground state structure has 1:2 ordering of Mg and Ta cations along the [111] direction of the cubic perovskite unit cell. The other phases with the next lowest electrostatic energy (Figs.3(b)-(d)) can be viewed as periodically “anti-phased” versions of the 1:2 ordering along the [111] direction. The structure of Fig.3(b), for example, contains segments of 1:2 ordering which are shifted along [111] every third cubic unit cell. Fig.3(c) is similar. It contains alternating [111] and [$\bar{1}\bar{1}\bar{1}$] versions of the 1:2 ordering.

The electrostatics of the system seems to prefer this defected [111] stacking to a perfect 1:2

stacking along any other direction. We calculated the electrostatic energy of a 1:2 ordering along the [100] direction, shown in Fig.3(e), and found it to rank 2062nd out of all 2194 cells investigated in terms of electrostatic energy.

3.2. First principles energy calculations

To investigate the dependence of the energy on the B-site ordering more quantitatively, we calculated the formation energy of 46 structures with different B-site arrangements by the *ab initio* pseudopotential method. The result is shown in Fig.4. The convex hull connecting the structures with lowest formation energies is also drawn in this figure to indicate the most stable phases among those considered with the pseudopotential method. The lowest energy structure has 1:2 ordering of Mg and Ta cations along the [111] direction in agreement with experimental observation. The calculated lattice parameters and ionic positions are shown in Table I. As is customary in the LDA, all lattice parameters are slightly smaller than the experimental ones. However, the calculated *c*/*a* axis ratio (7.029/5.727 = 1.227) is very good agreement with the experimental one (7.095/5.773 = 1.229)[34].

3.3. Cluster expansions and Monte Carlo simulations

A cluster expansion containing 14 terms for the $Ba(Mg_x,Ta_{1-x})O_3$ system is constructed by applying an inversion method based on linear programming techniques to the first-principles energies. This includes effective interactions corresponding to the empty cluster V_0, one point cluster, 7 pair clusters, 4 triplet clusters and one 5-pt cluster, as illustrated in Fig.5. The values of the ECI are shown in Fig.6 and listed in Table III. The comparison between the first-principles formation energies and cluster expansion fitted energies is also summarized in Fig.7. Since the cluster expansion can be implemented to calculate the energy of any configuration, we used it to estimate the energy difference

between the 1:2 ordered structure and the ideal disordered phase. The resulting value is 334 meV per perovskite unit. This indicates a large stability of the ordered structure with respect to the disordered arrangement. A more detailed temperature dependence characterization for the degree of this order can be studied by performing a Monte Carlo simulation on the results of the cluster expansion.

All Monte Carlo simulations are applied in a canonical ensemble on cells containing 24^3=13,824 B-sites. One thousand equilibration passes per lattice site are performed at each temperature, after which sampling occurred for 10,000 Monte Carlo passes. Figs.8 shows the internal energy as a function of temperature. The ordered phase clearly transforms to a disordered phase by a first order transition around 3770 K. The temperature dependence of the long-range 1:2 order (LRO) parameter η is evaluated from the Monte Carlo results and confirms the strong first order character of the transition (Fig.9). The LRO parameter η of the 1:2 B-site arrangements is estimated with perfect sublattices of Mg and Ta atoms, and normalization of valencies as:

$$h = \frac{\left(2 \times Mg_{s\_Mg} + Ta_{s\_Ta}\right) - \left(Ta_{s\_Mg} + 2 \times Mg_{s\_Ta}\right)}{\frac{4}{3} \times N} \quad , \qquad \text{(Eq.5)}$$

where A_{s_B} is the number of A atoms in the sublattice of B atoms and N is the total number of atoms. The BMT system has virtually no equilibrium disorder until it completely disorders at 3770 K.

Conventionally, $Ba(Mg_{1/3},Ta_{2/3})O_3$ is sintered at ~ 1923 K, and prolonged sintering or annealing at just below the transition temperature has been used to improve ordering[15,16]. However, our theoretical investigation suggests that sintering at higher temperatures for longer times or prolonging the annealing is effective in enhancing the degree of cation order in $Ba(Mg_{1/3},Ta_{2/3})O_3$, since our results indicate that equilibrium corresponds to a fully ordered material.

The order-disorder transformation temperature can depend sensitively on the accuracy of the cluster expansion. To acquire some information on possible errors in the cluster expansion, we tried to

obtain a direct energy evaluation of the disordered state to compare with the number predicted by the cluster expansion. Although a completely disordered structure can not be calculated as it has no translational symmetry, the disordered state can be approximated with Special Quasi-random Structures (SQS)[35]. These structures give the best possible approximation to a disordered state within a supercell of a given number of sites. The quality of the approximation is measured by how well the lattice correlations correspond to those of the disordered state. The correlations of the ideally disordered state are compared to those of the SQS we used (with nine B-sites) in Table II. The calculated energy difference between the 1:2 ordered state and the SQS is 311 meV/cell, which compares excellently with the cluster expansion result of 334 meV/cell. This may indicate that our cluster expansion is reasonably well converged.

3.4. Crystallographic details of the first principles calculated ground state

We have investigated the relaxation of the ions in the 1:2 ordered phase. Figs.10 and 11 respectively show the relaxation of the oxygen octahedron around the B-site cations and the interplanar distances from the ideal perovskite case. The results of the first-principles calculations indicate that ordering in a 1:2 arrangement along the [111] direction leads to the expansion of Mg-O octahedron (Distance of Mg-O: 2.100 Å) and contraction of Ta-O octahedron (Distance of Ta-O(I): 1.914 Å and of Ta-O(II): 2.068 Å) as shown in Fig.10(a). The experimental observation of an octahedron twist or distortion has been reported in some complex perovskite microwave ceramics[36,37] and Desu *et al*. pointed out that this kind of distortion was more significant than B-site ordering to improve microwave Q-factors[3]. According to these positional variations, the distance between the Mg layer and Ta layer is 3% smaller than that between Ta layers as illustrated in Fig.10(b).

To study details of bonding in $Ba(Mg_{1/3},Ta_{2/3})O_3$, we calculated the valence charge density.

The charge density distribution of the (110) plane in the primitive perovskite unit are shown in Fig.11 for the ground state. The charge density results seem to indicate that there is some bonding between Ta and O atoms. Mg is fully ionized and does not engage in covalent bonding with oxygen.

The density of states (DOS) for the $Ba(Mg_{1/3},Ta_{2/3})O_3$ ordered structure is plotted in Fig.12(a). The projected DOS for each element are given in Figs.12(b)-(e). As can be seen in Figs.12(d) and (e), there is some overlap between the O-2*p* orbitals, which are about 3 eV below the Fermi energy, and the Ta-5*d* orbitals, corresponding the results of charge density distribution.

4. Conclusion

In this work, the B-site cation ordering of $Ba(Mg_{1/3},Ta_{2/3})O_3$ microwave dielectrics with the complex perovskite structure has been studied using a combination of first-principles calculations, a cluster expansion technique, and Monte Carlo simulations. Our calculations confirm the experimentally observed hexagonal superstructure with space group $P\dot{3}m1$ (D^3_{3d}) as the ground state. The order-disorder transition between the low-temperature 1:2 ordered hexagonal phase ($P\dot{3}m1$) and high-temperature simple perovskite phase (Pm3m) is predicted to occur at ~ 3770 K. This indicates that $Ba(Mg_{1/3},Ta_{2/3})O_3$ in equilibrium should be fully ordered at all practical temperatures. Sintering at high temperature for a long time or prolonging the anneal should therefore be effective in enhancing the degree of cation order in $Ba(Mg_{1/3},Ta_{2/3})O_3$. The charge density distribution and one electron density of states (DOS) for the 1:2 ordered structure indicate that Ta and O atoms possess some degree of covalency and some overlap between the O-2*p* orbitals and the Ta-5*d* orbitals.

Also, the electrostatic stability of $Ba(Mg_{1/3},Ta_{2/3})O_3$ has been investigated using Madelung energy calculations for different B-site arrangements. This result shows the importance of 1:2 ordering of Mg and Ta cations along the [111] direction of the simple perovskite in determining electrostatic

stability of $Ba(Mg_{1/3},Ta_{2/3})O_3$.

Acknowledgments

This work was supported by the Department of energy, Office of Basic Energy Sciences under Contract No. DE-FG02-96ER45571. The authors would like to express their gratitude to Prof. W. Craig Carter of the Massachusetts Institute of Technology for generously providing us with his computing resources and S. K. Mishra of the Massachusetts Institute of Technology for his helpful advice. T. T. wishes to thank Taro Miura of TDK Techno Corporation, Hideaki Ninomiya and Shigekazu Sumita of TDK Corporation for their encouraging support. E. J. W. and A. V. D. V. gratefully acknowledge support from the National Science Foundation Graduate Research Fellowship Program and the DOE Computational Science Graduate Fellowship Program, respectively.

References

1) S. Nomura, K. Toyama and K. Kaneta : Jpn. J. Appl. Phys. **21** [10] (1982) 624.

2) S. Kawashima, M. Nishida, I. Ueda and H. Ouchi : J. Am. Ceram. Soc. **66** (1983) No.6, 421.

3) S. B. Desu and H. M. O'Bryan : J. Am. Ceram. Soc. **68** (1985) No.10, 546.

4) K. Wakino, D. A. Sagala and H. Tamura : Jpn. J. Appl. Phys. **24** (1985) No.Sup.24-2, 1042.

5) H. Tamura, D. A. Sagala and K. Wakino : Jpn. J. Appl. Phys. **25** (1986) No.6, 787.

6) T. Nagai, M. Sugiyama, M. Sando and K. Niihara : Jpn. J. Appl. Phys. **36** (1997) No.3A, 1146.

7) L. Chai and P. Davies : J. Am. Ceram. Soc. **80** (1997) No.12, 3193.

8) D. A. Sagala and S. Nambu : J. Phys. Soc. Jpn. **61** (1992) No.5, 1791.

9) R. McCormack and B. P. Burton : Comp. Mater. Sci. **8** (1997) 153.

10) R. McCormack and B. P. Burton : *Mater. Res. Soc. Symposium Proc.* **453** (1997) 449.

11) L. Bellaiche and D. Vanderbilt : Phys. Rev. Lett. **81** (1998) No.6, 1318.

12) T. Miura, T. Takahashi and M. Kobayashi : Inst. Electron. Inf. & Commun. Eng. Trans. Electron. **E77-C** (1994) No.6, 900.

13) T. Takahashi, Y. Iijima, M. Kobayashi and T. Miura : Jpn. J. Appl. Phys. **33** (1994) No.9B, 5510.

14) T. Takahashi, Y. Iijima and T. Miura : *IEEE Microwave Theory Tech. Symposium Digest* (1997) 1638.

15) K. Matsumoto, T. Hiuga, K. Takada and H. Ichimura : *IEEE International Symposium on Applications of Ferroelectrics Digest* (1986) 118.

16) H. Matsumoto, H. Tamura and K. Wakino : Jpn. J. Appl. Phys. **30** (1991) No.9B, 2347.

17) K. Wakino : Ferroelectrics **91** (1989) 69.

18) F. Galasso, J. R. Barrante and L. Katz : J. Am. Chem. Soc. **83** (1961) 2830.

19) F. Galasso and J. Pyle : Inorg. Chem. **2** (1963) No.3, 482.

20) J. M. Sanchez, F. Ducastelle and D. Gratias, Physica A **128** (1984) 334.

21) F. Ducastelle : "*Order and Phase Stability in Alloys*" (Kluwer-Dordrecht, Amsterdam, 1990).

22) D. de Fontaine : Solid State Phys. **47** (1994) 33.

23) G. Ceder : "*Encyclopedia of Advanced Materials*", ed. D. Bloor, R. J. Brook, M. C. Flemings and S. Mahajan (Pergamon, New York, 1994) 1951.

24) G. Ceder, A. F. Kohan, M. K. Aydinol, P. D. Tepesch and A. Van der Ven : J. Am. Ceram. Soc. **81** (1998) 517.

25) A. Van der Ven, M. K. Aydinol and G. Ceder : Phys. Rev. B **58** (1998) 2975.

26) G. D. Garbulsky and G. Ceder : Phys. Rev. B **51** (1995) 67.

27) K. Binder and D. W. Heermann : "*Monte Carlo Simulation in Statistical Physics*" (Springer-Verlag, Berlin, 1988).

28) G. Kresse and J. Furthmüller : Phys. Rev. B **54** (1996) No.11, 169.

29) G. Kresse and J. Furthmüller : Comp. Mater. Sci. **6** (1996) 15.

30) D. Vanderbilt : Phys. Rev. B **41** (1990) 7892.

31) G. Kresse and J. Hafner : J. Phys. Condens. Matter **6** (1994) 8245.

32) D. M. Ceperley and B. J. Alder : Phys. Rev. Lett. **45** (1980) 566.

33) J. P. Perdew and A. Zunger : Phys. Rev. B **23** (1981) 5048.

34) H. Vincent, C. Perrier, P. l'Heritier and M. Labeyrie : Mater. Res. Bull. **28** (1993) No.9, 951.

35) A. Zunger, S.-H. Wei, L. Ferreira and J. E. Bernard : Phys. Rev. Lett. **65** (1990) 353.

36) J. Kato, M. Fujii, H. Kagata and K. Nishimoto : Jpn. J. Appl. Phys. **32** (1993) No.9B, 4356.

37) J. Joseph, T. M. Vimala, K. C. J. Raju and V. R. K. Murthy : Jpn. J. Appl. Phys. **35** (1996) No.1A, 179.

Figures

Fig.1(a) Crystal structure of disordered $Ba(Mg_{1/3},Ta_{2/3})O_3$ as a simple perovskite cell with space group Pm3m (O^1_h).

Fig.1(b) B-site stacking sequence of the ordered $Ba_3(Mg,Ta_2)O_9$ structure.

Fig.1(c) Crystal structure of ordered $Ba_3(Mg,Ta_2)O_9$ as a hexagonal superlattice with space group $P\bar{3}m1$ (D^3_{3d}).

Fig.2 Crystal structures of $Ba(Mg_{1/3},Ta_{2/3})O_3$ supercells corresponding to the four lowest Coulomb energies for a fixed lattice of Mg and Ta ions ($E_a < E_b < E_c < E_d$).

Fig.3 B-site configurations of $Ba(Mg_{1/3},Ta_{2/3})O_3$ supercells with (a) first lowest, (b) second lowest, (c) third lowest, (d) fourth lowest, and (e) two-thousand-sixty-second lowest Madelung energy.

Fig.4 Formation energies of 46 different B-site configurations in $Ba(Mg_x,Ta_{1-x})O_3$ system calculated with the pseudopotential method.

Fig.5 Clusters used in the cluster expansion technique.

Fig.6 Values of the Effective Cluster Interactions (ECI).

Fig.7 Comparison between first principles formation energies (ð) and cluster expansion fitted energies (+).

Fig.8 Energy in the Monte Carlo simulation as a function of temperature.

Fig.9 Long-range 1:2 order parameter η as a function of temperature.

Fig.10(a) Octahedron distortions surrounding Mg and Ta cations for the calculated ground state.

Fig.10(b) B-site plane arrangement for calculated ground state.

Fig.11 Charge density distribution of the (110) plane of the primitive perovskite cell for ordered $Ba(Mg_{1/3},Ta_{2/3})O_3$.

Fig.12 One electron density of states (DOS) of the ordered $Ba(Mg_{1/3},Ta_{2/3})O_3$ structure for (a) total, (b)

Ba atom, (c) Mg atom, (d) Ta atom, and (e) O atom.

Table I. Atomic coordinates of the first-principles calculated ground state. Values in parentheses are reference positions in ideal perovskite structure.

a =5.727 (Å), *b*=5.727 (Å), *c*=7.029 (Å), α=90.00, β=90.00, γ=120.00

(Experimental: *a* =5.773 (Å), *b*=5.773 (Å), *c*=7.095 (Å), α=90.00, β=90.00, γ=120.00)[34)]

Element	Site	Atomic coordinate		
		X	Y	z
Ba	1a	0.0000	0.0000	0.0000
Ba	2d	0.3333	0.6667	0.6627 (0.6667)
Mg	1b	0.0000	0.0000	0.5000
Ta	2d	0.3333	0.6667	0.1767 (0.1667)
O	3e	0.5000	0.0000	0.0000
O	6i	0.1713 (0.1667)	0.8287 (0.8333)	0.3245 (0.3333)

Table II. Comparison of pair-cluster correlation functions between special quasi-dynamic structure (SQS) and ideal disordered structure.

Cluster type	Special Quasi-dynamic Structure	Ideal disordered structure
Point cluster	-0.333333	-0.333333
First NN Pair cluster	0.111111	0.111111
Second NN Pair cluster	0.111111	0.111111
Third NN Pair cluster	0.000000	0.111111
Fourth NN Pair cluster	0.111111	0.111111
Fifth NN Pair cluster	0.111111	0.111111
Sixth NN cluster	0.000000	0.111111
Seventh NN Pair cluster	0.111111	0.111111
Eighth NN Pair cluster	0.000000	0.111111
Ninth NN Pair cluster	1.000000	0.111111
Tenth NN Pair cluster	0.111111	0.111111
Eleventh NN Pair cluster	0.111111	0.111111
Twelfth NN Pair cluster	0.000000	0.111111
Thirteenth NN Pair cluster	0.111111	0.111111
Fourteenth NN Pair cluster	0.111111	0.111111
Fifteenth NN Pair cluster	0.111111	0.111111
Sixteenth-a NN Pair cluster	0.111111	0.111111
Sixteenth-b NN Pair	0.111111	0.111111
Eighteenth-a NN Pair	0.000000	0.111111
Eighteenth-b NN Pair	1.000000	0.111111
Twentieth NN Pair cluster	0.111111	0.111111

Table III. ECI of cluster expansions for formation energies.

Cluster type	Coordinate combination	V_α ECI (meV/cell)
Empty cluster V_0	------	-1717.542986
Point cluster	(000)	1414.742849
First NN Pair cluster	(000)-(100)	-30.093824
Second NN Pair cluster	(000)-(110)	0.936342
Third NN Pair cluster	(000)-(111)	57.324777
Fourth NN Pair cluster	(000)-(200)	121.953925
Fifth NN Pair cluster	(000)-(210)	61.502962
Sixth NN Pair cluster	(000)-(210)	33.867582
Eighth-b NN Pair cluster	(000)-(300)	20.866331
First NN triplet cluster	(000)-(100)-(101)	-67.282857
Second-a NN triplet cluster	(000)-(100)-(011)	-15.733278
Second-b NN triplet cluster	(000)-(110)-(010)	-16.416667
Second-c NN triplet cluster	(000)-(100)-(200)	9.389252
First-b NN 5-pt cluster	(100)-(110)-(111)-(010)-(001)	-21.709601

* Origin (000) is converted from referential B-site atomic position (1/2, 1/2, 1/2) in the primitive perovskite structure.

Fig.1(a)

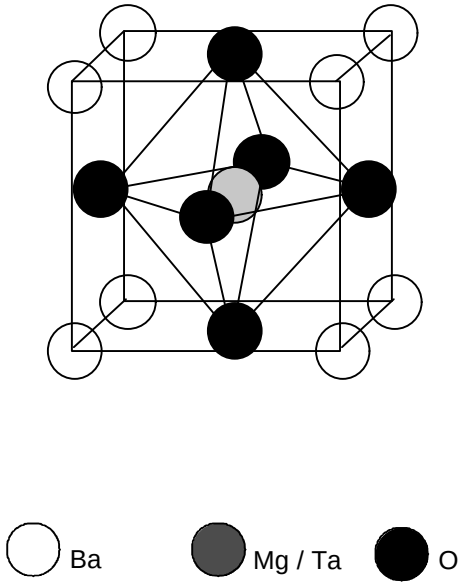

Fig.1(b)

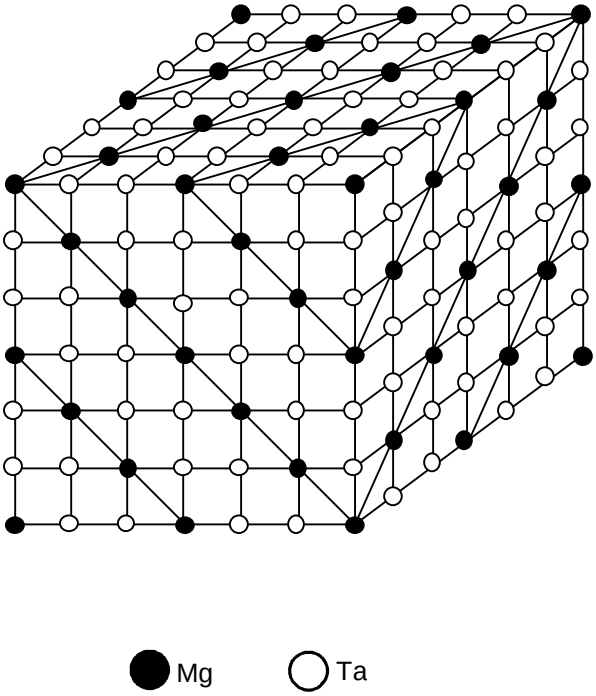

Fig.1(c)

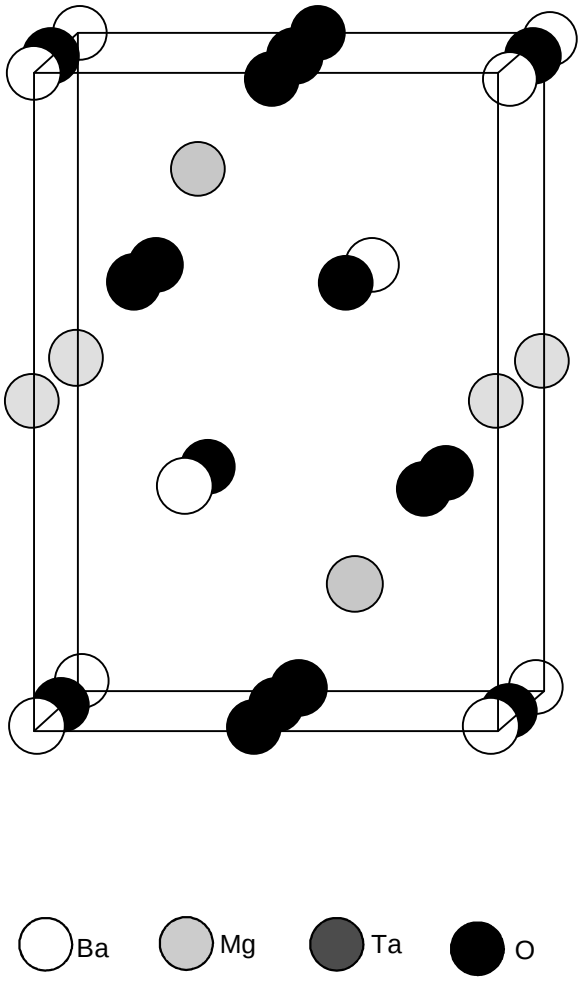

Fig.2(a)

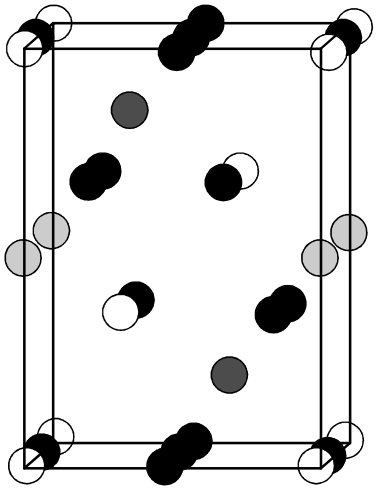

$P\bar{3}m1$

Fig.2(b)

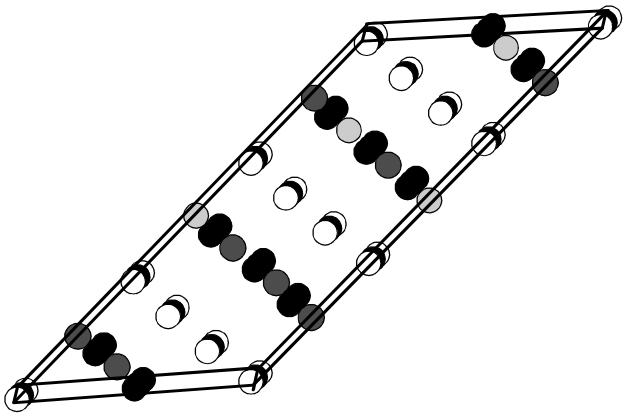

$C2/m$

Fig.2(c)

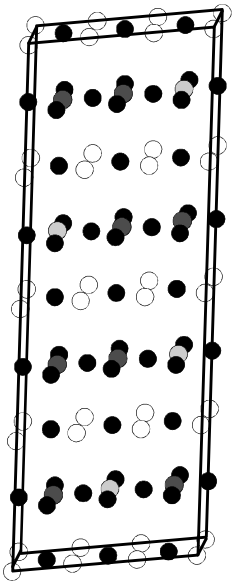

Cmcm

Fig.2(d)

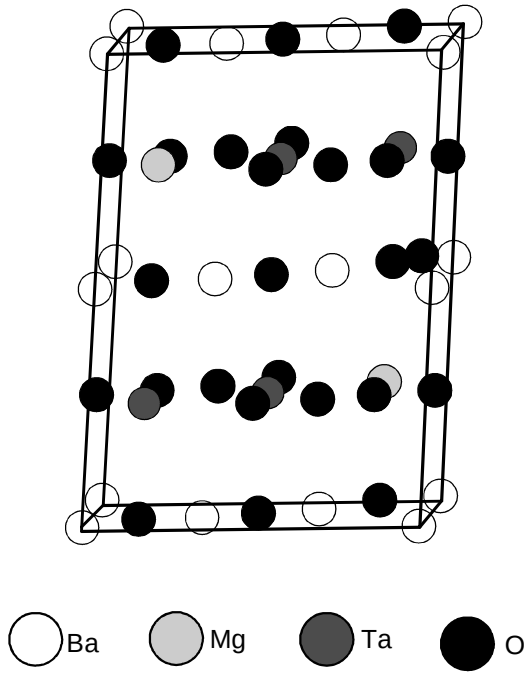

$P2_1/m$

Fig.3(a)

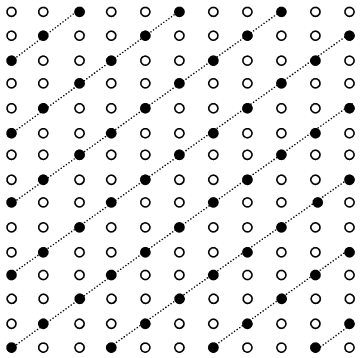

$P\bar{3}m1$

Fig.3(b)

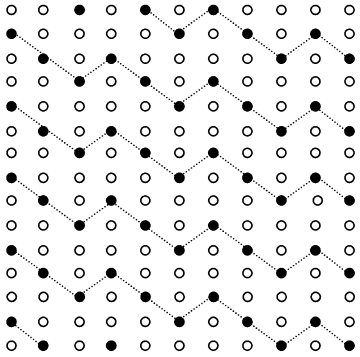

$C2/m$

Fig.3(c)

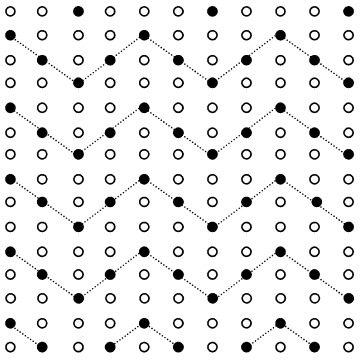

$Cmcm$

Fig.3(d)

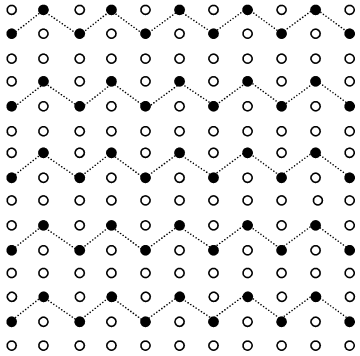

$P2_1/m$

Fig.3(e)

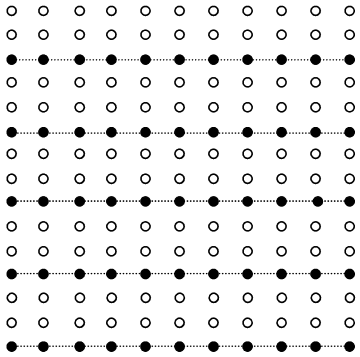

$P4/mmm$

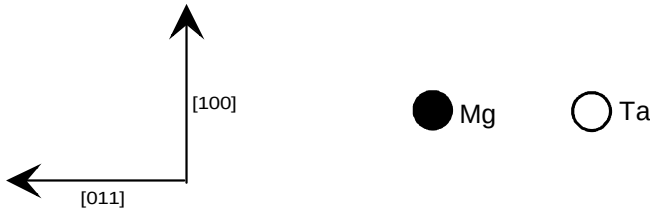

Fig.4

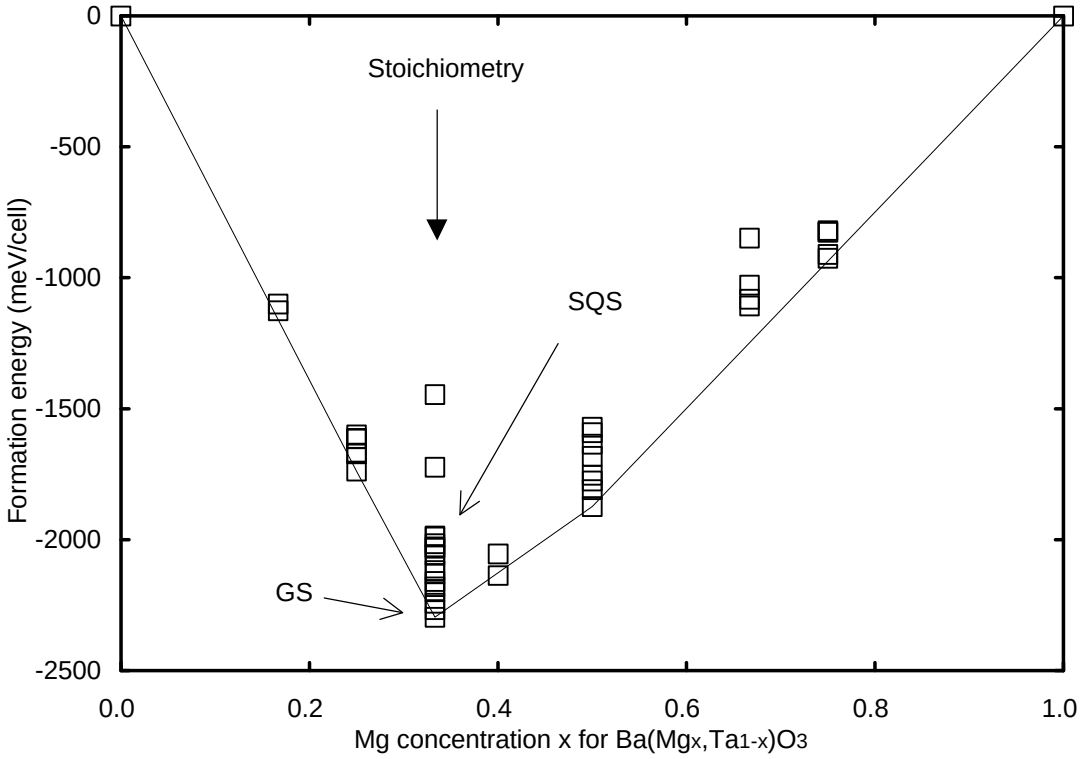
0
-500
-1000
-1500
-2000
-2500
Formation energy (meV/cell)
Stoichiometry
SQS
GS
0.0
0.2
0.4
0.6
0.8
1.0
Mg concentration x for Ba(Mgx,Ta1-x)O3

Fig.5

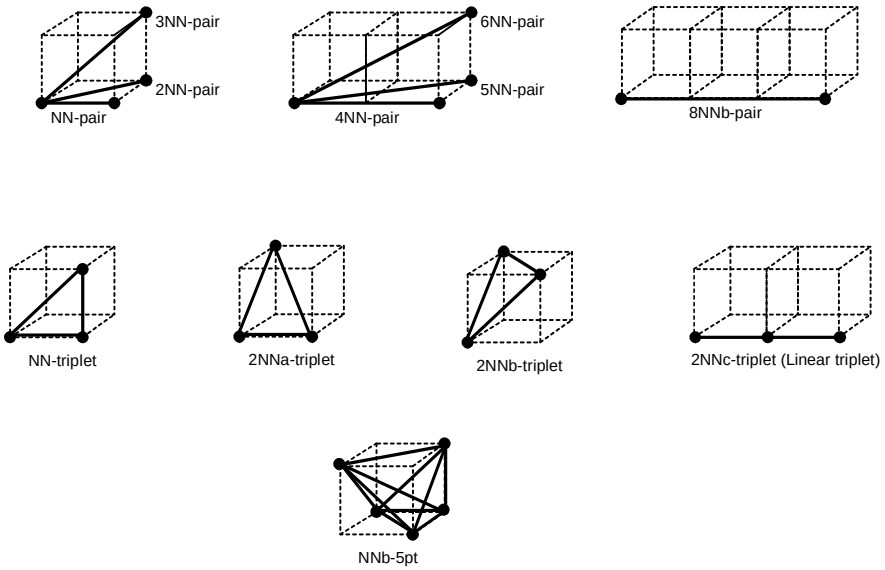
3NN-pair
2NN-pair
NN-pair
6NN-pair
5NN-pair
4NN-pair
8NNb-pair
NN-triplet
2NNa-triplet
2NNb-triplet
2NNc-triplet (Linear triplet)
NNb-5pt

Fig.6

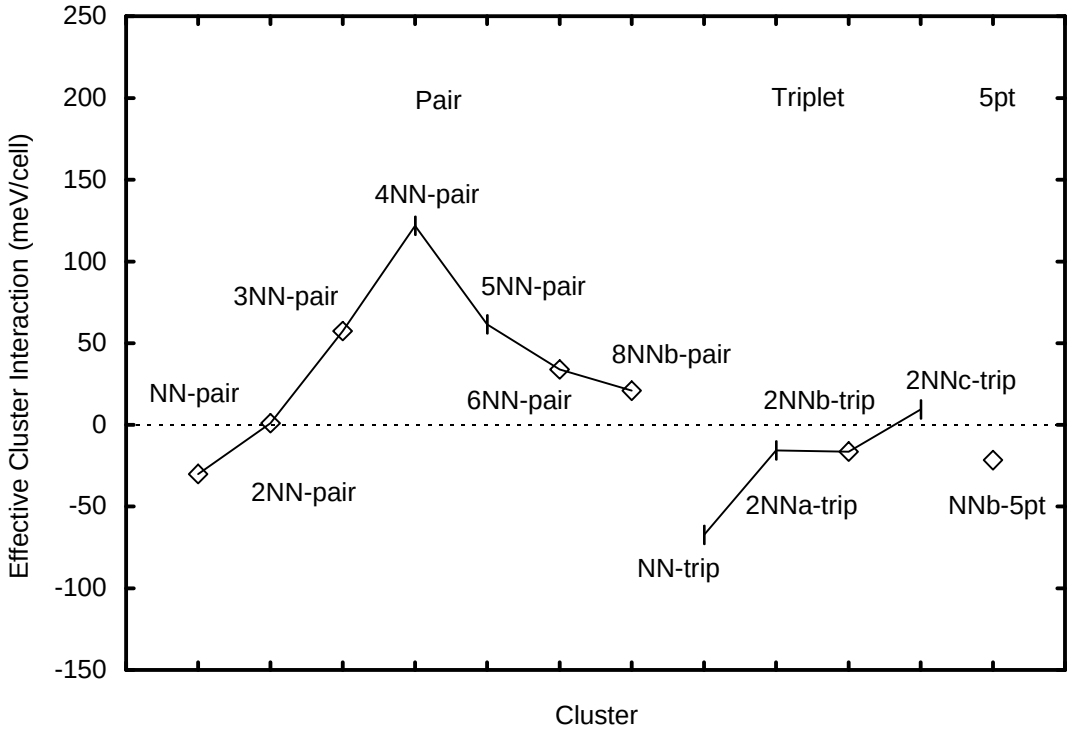
250
200
150
100
50
0
-50
-100
-150
Effective Cluster Interaction (meV/cell)
Cluster
Pair
Triplet
5pt
NN-pair
2NN-pair
3NN-pair
4NN-pair
5NN-pair
6NN-pair
8NNb-pair
NN-trip
2NNa-trip
2NNb-trip
2NNc-trip
NNb-5pt

Fig.7

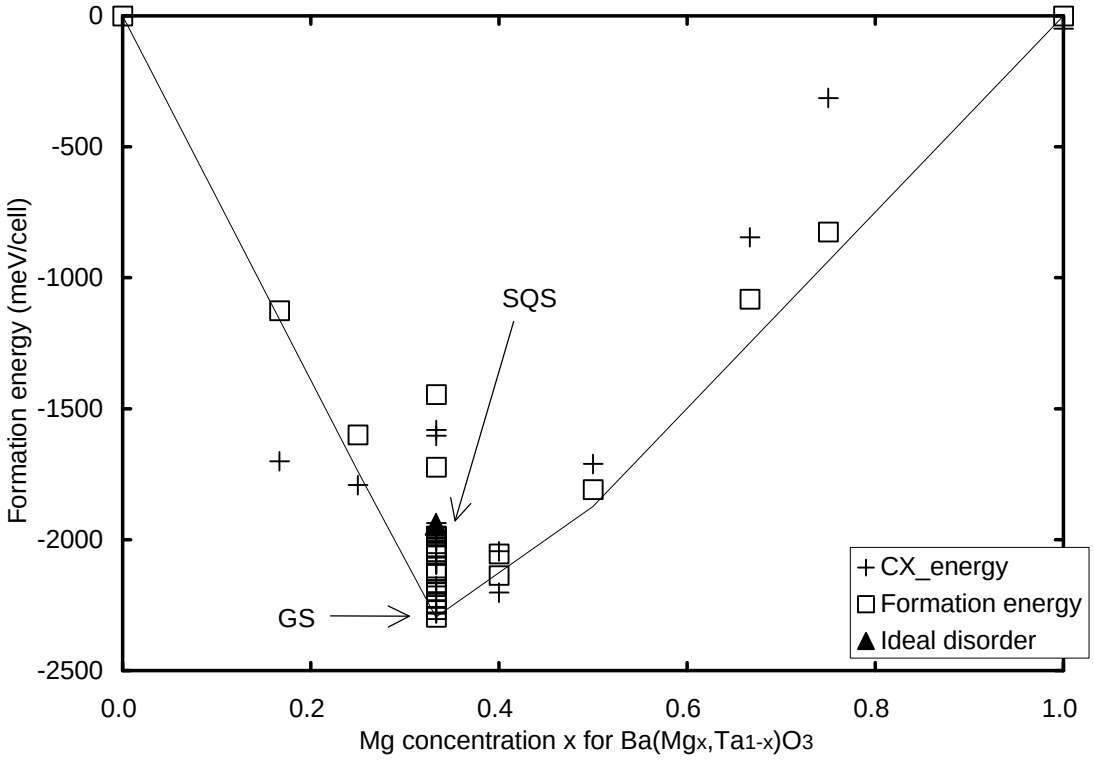
0
-500
-1000
-1500
-2000
-2500
Formation energy (meV/cell)
0.0
0.2
0.4
0.6
0.8
1.0
Mg concentration x for Ba(Mgx,Ta1-x)O3
SQS
GS
CX_energy
Formation energy
Ideal disorder

Fig.8

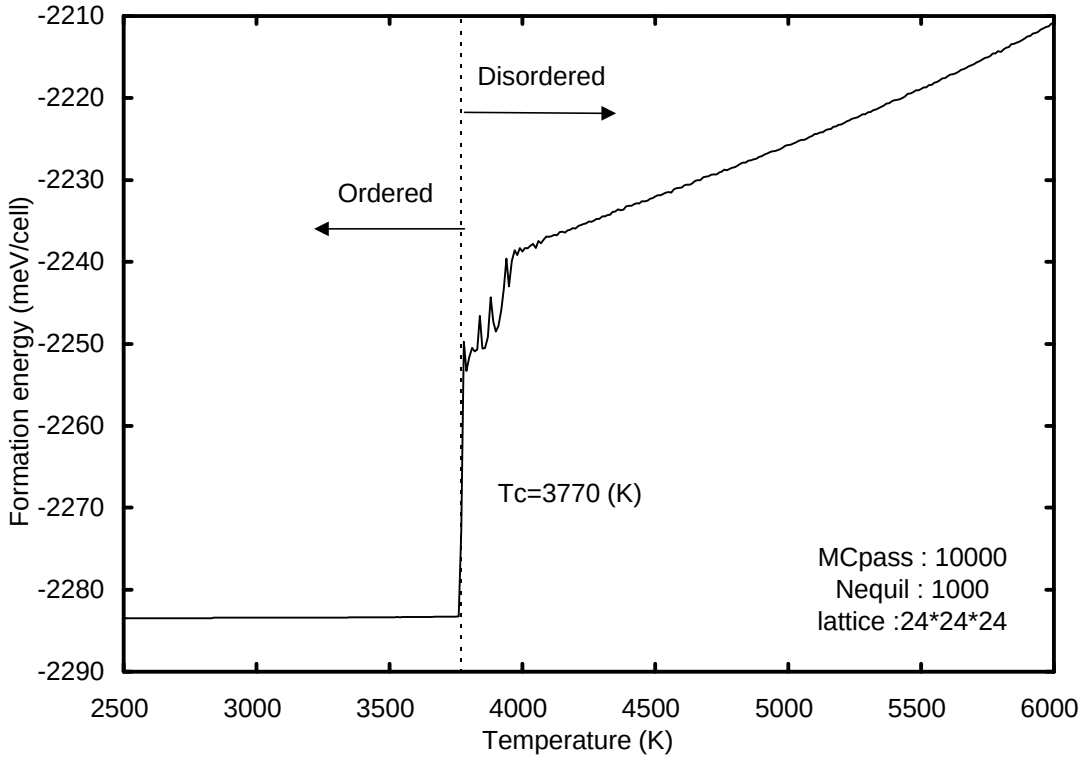
-2210
-2220
-2230
-2240
-2250
-2260
-2270
-2280
-2290
Formation energy (meV/cell)
2500
3000
3500
4000
4500
5000
5500
6000
Temperature (K)
Disordered
Ordered
Tc=3770 (K)
MCpass : 10000
Nequil : 1000
lattice :24*24*24

Fig.9

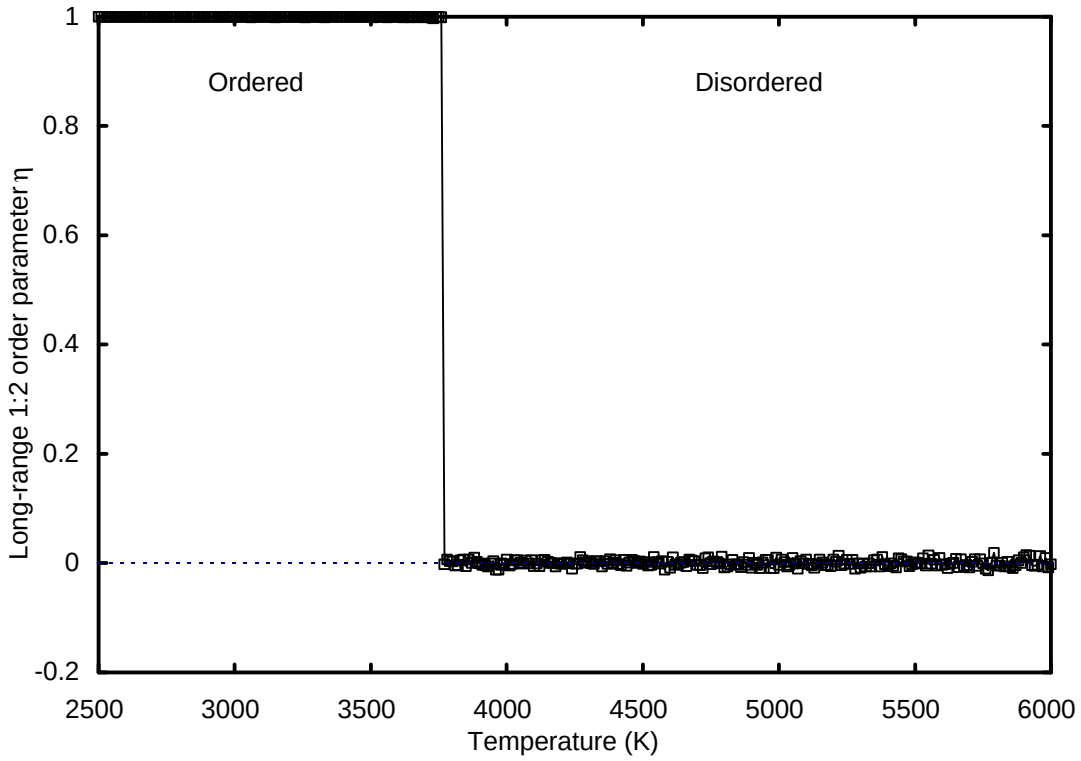
Ordered
Disordered
Long-range 1:2 order parameter η
Temperature (K)
1
0.8
0.6
0.4
0.2
0
-0.2
2500
3000
3500
4000
4500
5000
5500
6000

Fig.10(a)

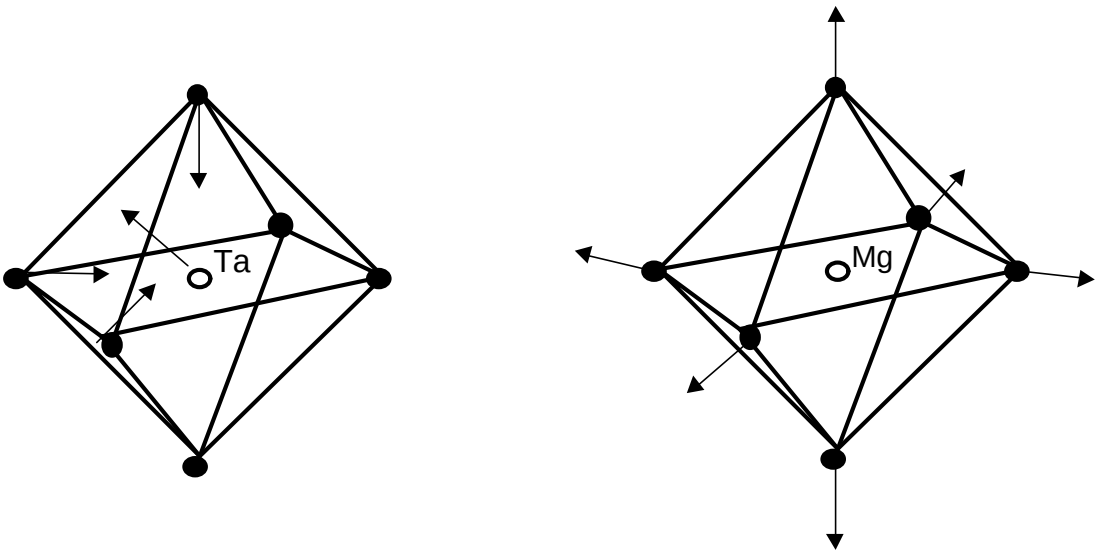

Fig.10(b)

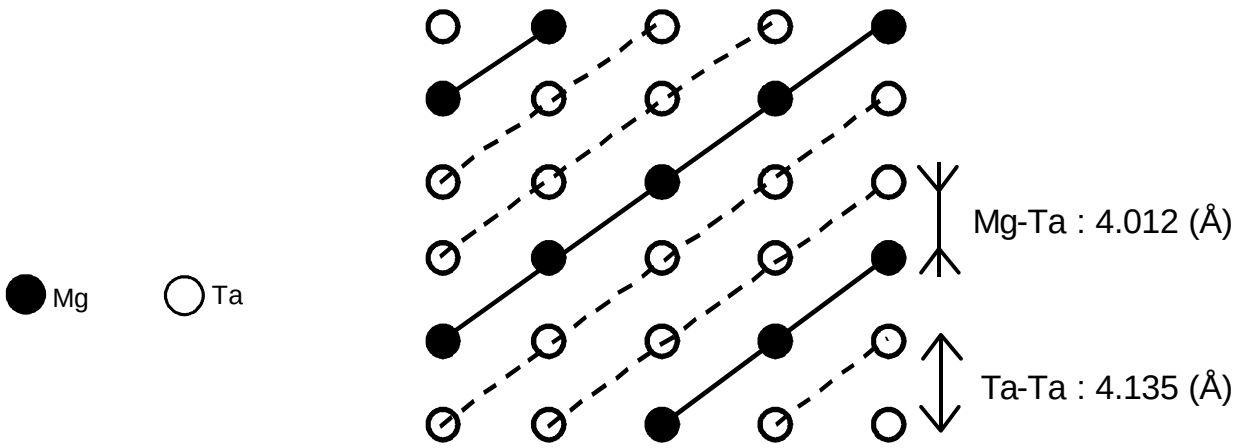

Fig.11

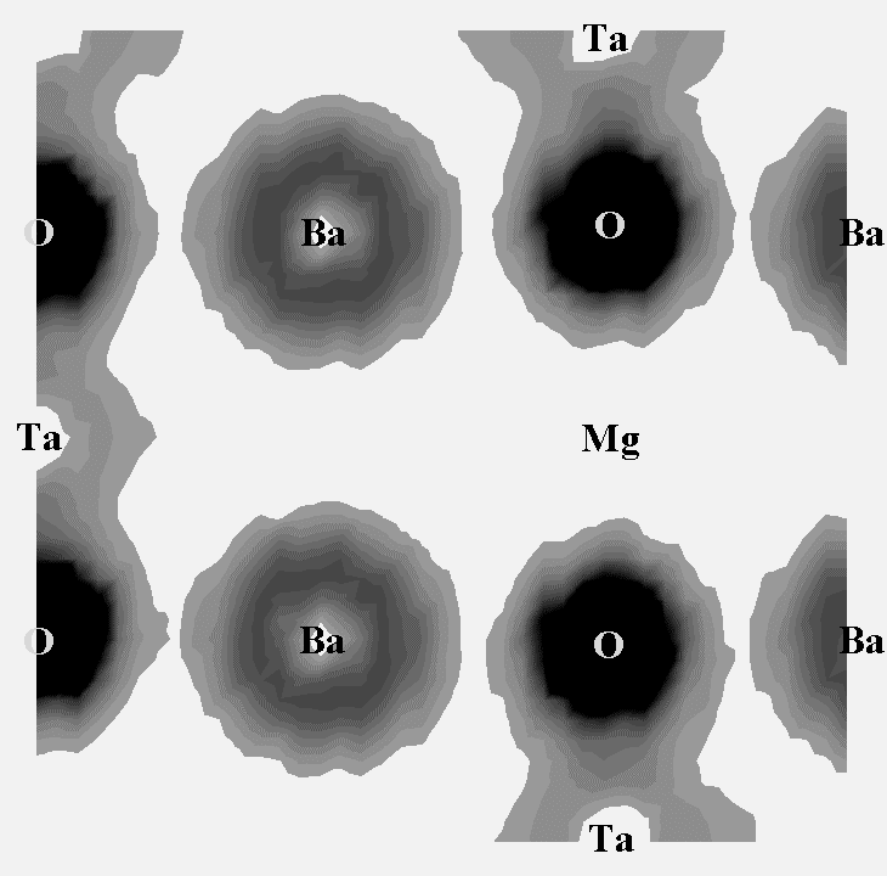

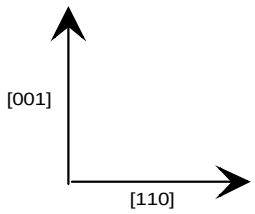

Fig.12(a)

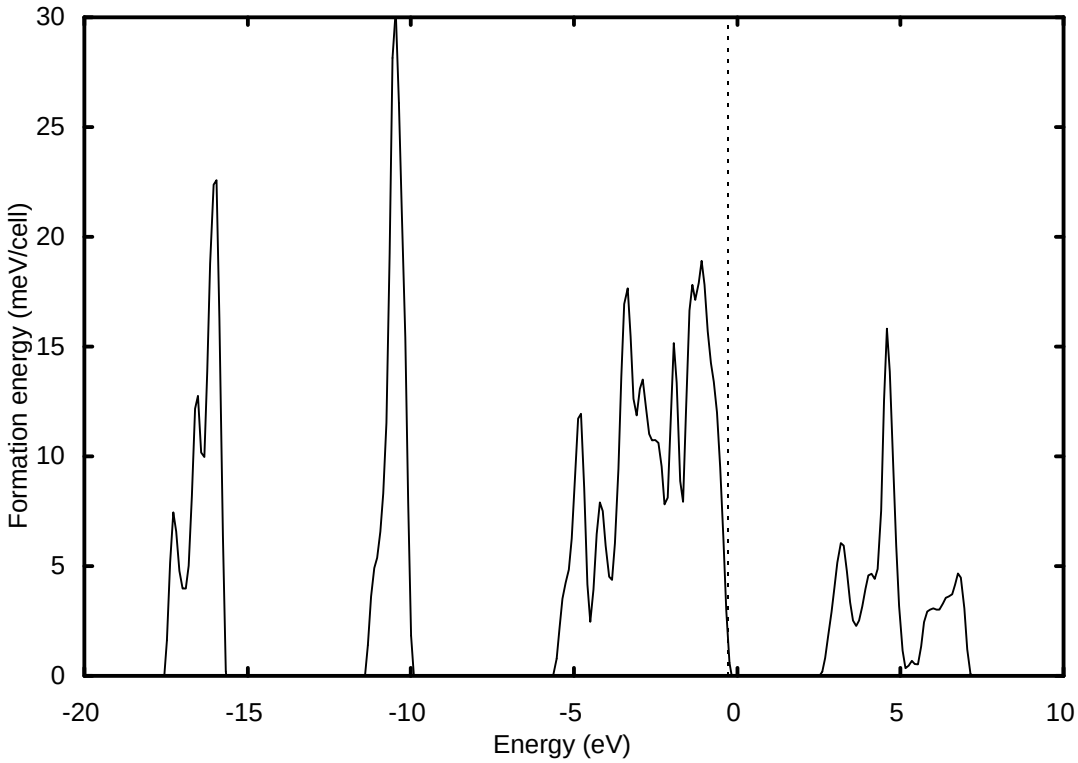
30
25
20
15
10
5
0
Formation energy (meV/cell)
-20
-15
-10
-5
0
5
10
Energy (eV)

Fig.12(b)

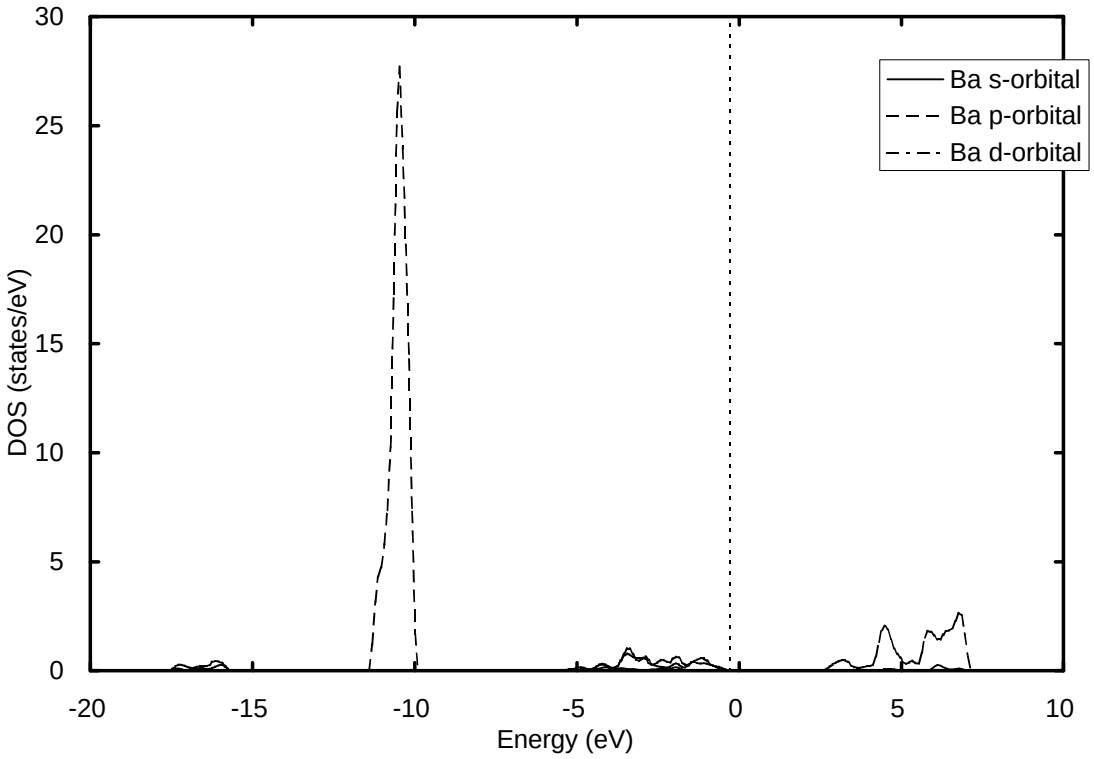
30
25
20
15
10
5
0
DOS (states/eV)
-20
-15
-10
-5
0
5
10
Energy (eV)
Ba s-orbital
Ba p-orbital
Ba d-orbital

Fig.12(c)

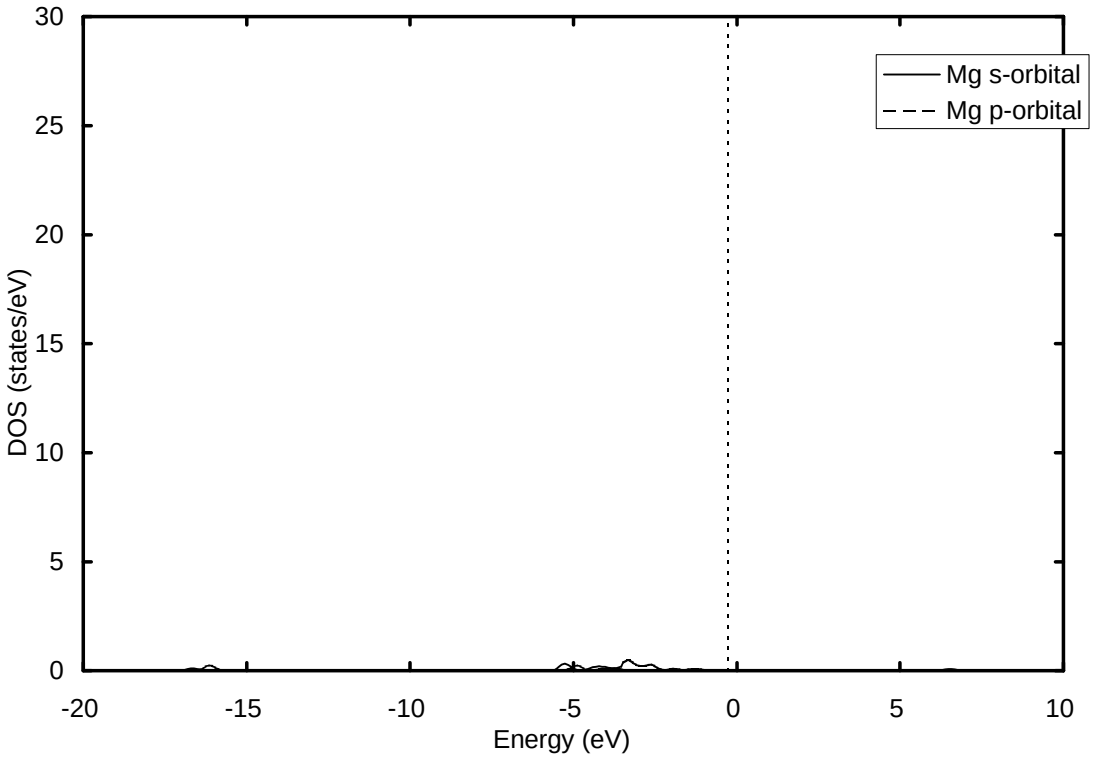
30
25
20
15
10
5
0
DOS (states/eV)
-20
-15
-10
-5
0
5
10
Energy (eV)
Mg s-orbital
Mg p-orbital

Fig.12(d)

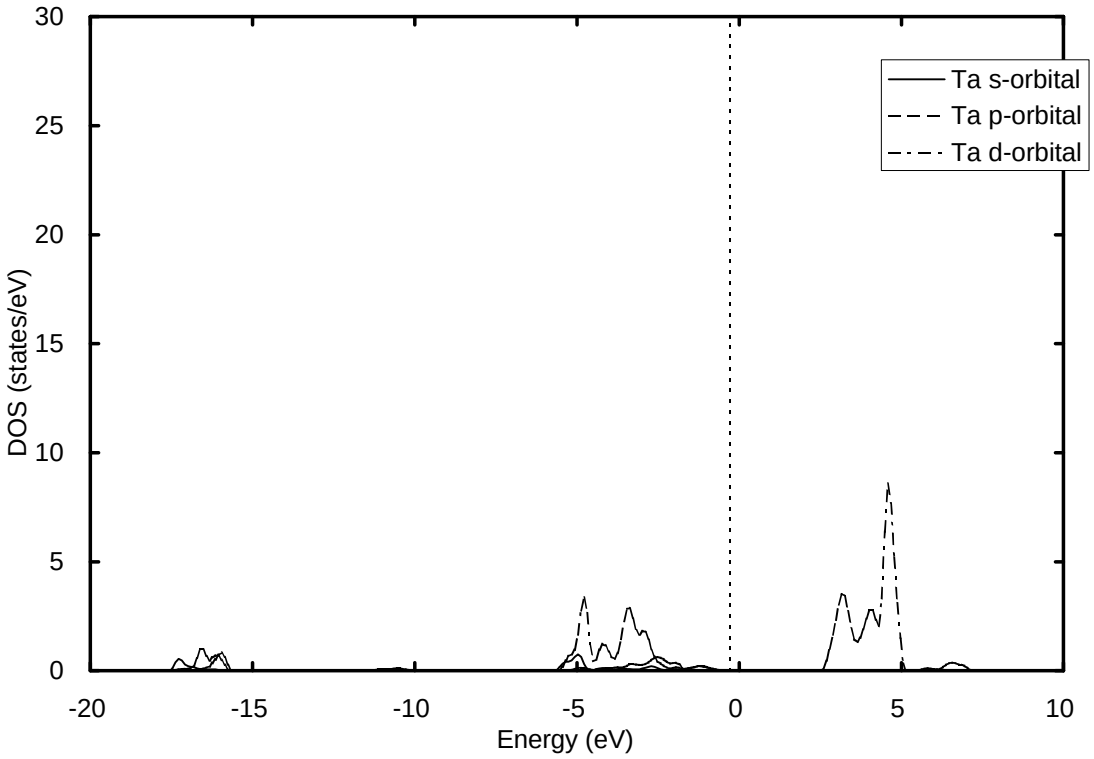
30
25
20
15
10
5
0
DOS (states/eV)
-20
-15
-10
-5
0
5
10
Energy (eV)
Ta s-orbital
Ta p-orbital
Ta d-orbital

Fig.12(e)

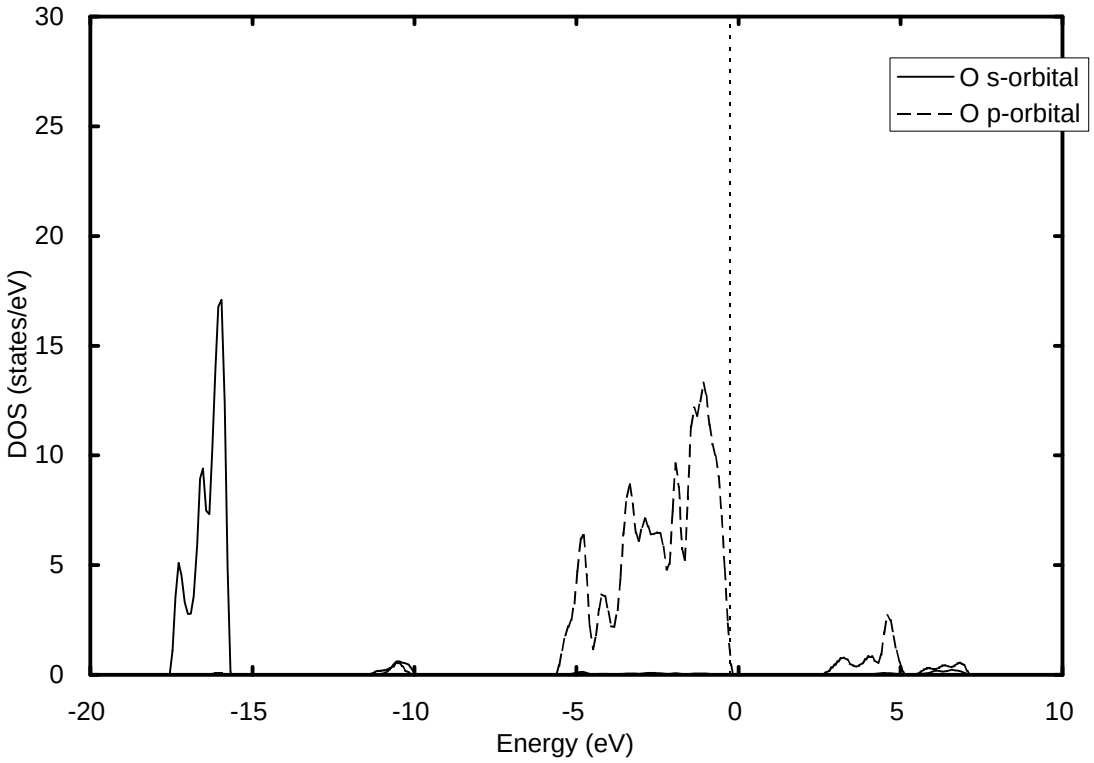
30
25
20
15
10
5
0
DOS (states/eV)
-20
-15
-10
-5
0
5
10
Energy (eV)
O s-orbital
O p-orbital